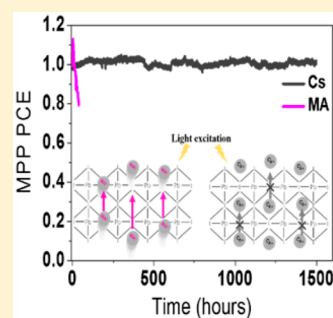


## Light-Independent Ionic Transport in Inorganic Perovskite and Ultrastable Cs-Based Perovskite Solar Cells

Wenke Zhou,<sup>†,#</sup> Yicheng Zhao,<sup>†,#</sup> Xu Zhou,<sup>†,§</sup> Rui Fu,<sup>†</sup> Qi Li,<sup>†</sup> Yao Zhao,<sup>†</sup> Kaihui Liu,<sup>†,‡</sup> Dapeng Yu,<sup>†,||</sup> and Qing Zhao<sup>\*,†,‡,||</sup><sup>†</sup>State Key Laboratory for Mesoscopic Physics and Electron Microscopy Laboratory, School of Physics, Peking University, Beijing 100871, China<sup>‡</sup>Collaborative Innovation Center of Quantum Matter, Beijing 100084, China<sup>§</sup>Academy for Advanced Interdisciplinary Studies, Peking University, Beijing 100871, China<sup>||</sup>Institute for Quantum Science and Technology and Department of Physics, South University of Science and Technology of China (SUSTech), Shenzhen 518055, China

## S Supporting Information

**ABSTRACT:** Due to light-induced effects in CH<sub>3</sub>NH<sub>3</sub>-based perovskites, such as ion migration, defects formation, and halide segregation, the degradation of CH<sub>3</sub>NH<sub>3</sub>-based perovskite solar cells under maximum power point is generally implicated. Here we demonstrated that the effect of light-enhanced ion migration in CH<sub>3</sub>NH<sub>3</sub>PbI<sub>3</sub> can be eliminated by inorganic Cs substitution, leading to an ultrastable perovskite solar cell. Quantitatively, the ion migration barrier for CH<sub>3</sub>NH<sub>3</sub>PbI<sub>3</sub> is 0.62 eV under dark conditions, larger than that of CsPbI<sub>2</sub>Br (0.45 eV); however, it reduces to 0.07 eV for CH<sub>3</sub>NH<sub>3</sub>PbI<sub>3</sub> under illumination, smaller than that for CsPbI<sub>2</sub>Br (0.43 eV). Meanwhile, photoinduced halide segregation is also suppressed in Cs-based perovskites. Cs-based perovskite solar cells retained >99% of the initial efficiency (10.3%) after 1500 h of maximum power point tracking under AM1.5G illumination, while CH<sub>3</sub>NH<sub>3</sub>PbI<sub>3</sub> solar cells degraded severely after 50 h of operation. Our work reveals an uncovered mechanism for stability improvement by inorganic cation substitution in perovskite-based optoelectronic devices.



Organic–inorganic hybrid perovskite solar cells (PSCs) exhibited a 22.1% record certified efficiency recently,<sup>1</sup> while the long-term stability issue still remains as an Achilles heel for their commercialization. Among the high-performance PSCs,<sup>2–8</sup> [methylammonium (MA)/formamidinium (FA)]<sup>+</sup> and [PbI<sub>3</sub>]<sup>−</sup> constitute the matrix to fabricate high-quality crystal films; however, the corresponding devices still degrade at the maximum power point (MPP) under illumination even with a UV filter. This issue is supposed to relate to material decomposition and ion migration in the perovskites.<sup>9–19</sup> Although the material itself passes the damp heat stability test,<sup>20</sup> fast degradation behavior is still observed at the early stage, the so-called “burn-in” degradation, implying ion migration-related destruction in devices. Recently, the Cs-enhanced crystal structure of perovskites was manifested by thermal stability, humidity resistance, and photostability,<sup>3,21–25</sup> however, a detailed study is still lacking on whether the ion migration can be tailored by Cs incorporation in perovskites. It is, therefore, valuable to compare the ionic transport for MA- and Cs-based perovskites, under dark and illumination.

We mainly focused on MAPbI<sub>3</sub> and CsPbI<sub>2</sub>Br perovskite films by taking the thermal/ambient phase stability and bandgap (1.92 eV) into consideration.<sup>22,23,26,27</sup> The corresponding ion migration barriers in both MAPbI<sub>3</sub> and CsPbI<sub>2</sub>Br thin films are extracted by analyzing cryogenic galvanostatic<sup>28–30</sup> and

current–voltage experiments in Au/perovskite (MAPbI<sub>3</sub> or CsPbI<sub>2</sub>Br)/Au lateral structures over various temperatures (100–295 K) and light intensities (0.1–25 mW/cm<sup>2</sup>). For MAPbI<sub>3</sub>, the ion migration energy barrier ( $E_a$ ) is reduced by approximately 1 order of magnitude (from 0.62 to 0.07 eV) when light illumination changes from 0.1 to 25 mW/cm<sup>2</sup>. However, the  $E_a$  CsPbI<sub>2</sub>Br is almost light-independent with 0.45 eV. Moreover, the related light-induced halide segregation in MA-based mixed-halide perovskites<sup>30,31</sup> is not detected in Cs-based perovskites. The halide stabilization is consistent with the light-independent nature in inorganic mixed-halide perovskites under strong illumination. For solar cell operation under AM1.5G illumination, the CsPbI<sub>2</sub>Br device presents <1% relative efficiency loss over 1500 h working at the MPP in a glovebox, while MAPbI<sub>3</sub> devices show a severe degradation within 50 h. Our work reveals the light-independent ion migration in Cs-based perovskites and highlights the necessity of maximizing Cs incorporation in high-efficiency PSCs to enhance the stability.

In our previous work on MAPbI<sub>3</sub>, light-enhanced ion migration could cause plane dendritic structures under high-field poling ( $\sim 2 \text{ V } \mu\text{m}^{-1}$ ) conditions in a Au/perovskite/Au lateral structure.<sup>30</sup>

Received: July 18, 2017

Accepted: August 17, 2017

Published: August 17, 2017

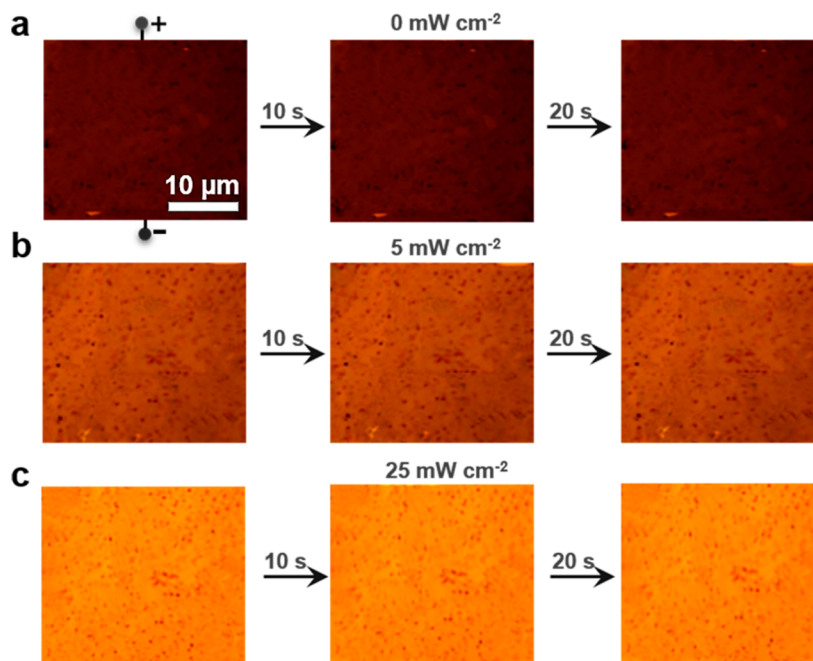


**Figure 1.** Monitoring of the optical images of a CsPbI<sub>2</sub>Br film during the poling process in ambient air at 25 °C: (a) in the dark, (b) under 5 mW/cm<sup>2</sup>, and (c) under 25 mW/cm<sup>2</sup>. The temperature variation of the perovskite films is less than 1 °C under illumination.

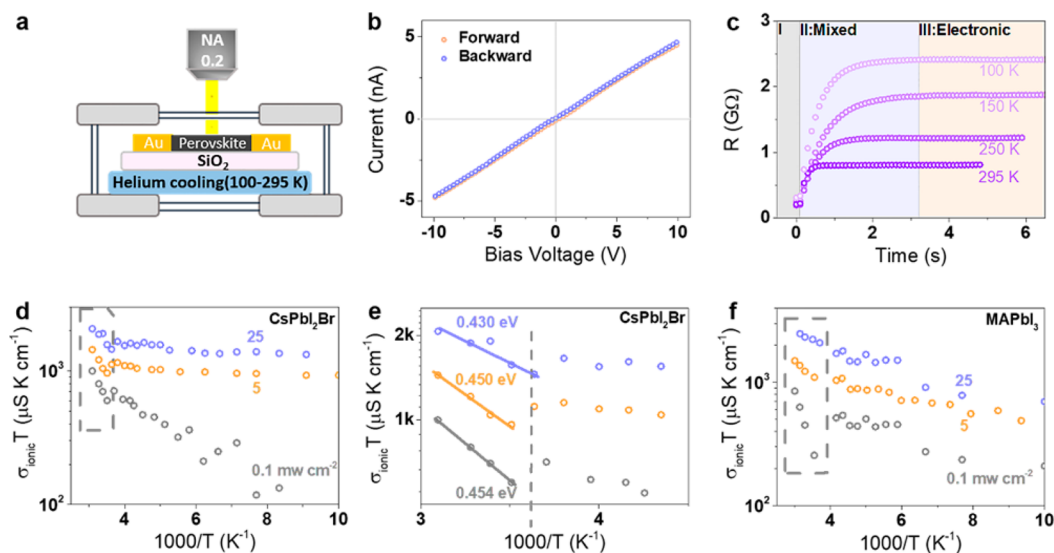


**Figure 2.** Cryogenic galvanostatic and current–voltage experiments in a Au/perovskite (MAPbI<sub>3</sub> or CsPbI<sub>2</sub>Br)/Au lateral structure. (a) Schematic illustration of the conductivity measurement setup. (b) Voltage–current ( $V$ – $I$ ) curves for the lateral device at 295 K under dark conditions. (c) Four typical galvanostatic curves at different temperatures under 5 mW/cm<sup>2</sup> illumination. A 0.1 nA current was switched on at 0.1 s. (d) Ionic conductivity of CsPbI<sub>2</sub>Br films,  $\sigma_{\text{ion}}T$ , under different light intensities. (e) Zoomed-in data of the dashed box in (d). (f) Ionic conductivity of MAPbI<sub>3</sub> films  $\sigma_{\text{ion}}T$ , under different light intensities.

However, with CsPbI<sub>2</sub>Br in the same structure (Figures S1 and S2a,b), the dendritic structure is not observed under illumination (5 and 25 mW/cm<sup>2</sup>) for 20 s (Figure 1). The above results indicate either a large ion migration barrier under illumination or that light-independent ion migration exists in Cs-based perovskite films, compared to MA-based perovskite films. To examine whether the halide anion also plays a critical role here, we further investigate MAPbBr<sub>3</sub> (Figure S2c) and MAPb(I<sub>0.9</sub>Br<sub>0.1</sub>)<sub>3</sub> (Figure S2d) perovskite thin films for poling experiments. Similar to MAPbI<sub>3</sub>, plane dendritic structures are observed under illumination (Figure S3), excluding the influence of a halide (I/Br) ratio change.

To obtain the ion migration barrier for CsPbI<sub>2</sub>Br and MAPbI<sub>3</sub> films, we combine cryogenic galvanostatic with voltage–current measurements (Figure 2a) to extract the energy barrier under a varying light intensity. The energy barrier of ion migration ( $E_a$ ) can be derived from eq 1<sup>32</sup>

$$\begin{aligned} \sigma_{\text{ion}}(T)T &= n e \mu = \frac{Z_i e^2 N_A C_v D_0}{k_B V_m} \exp\left(-\frac{G_v}{S k_B T}\right) \exp\left(-\frac{E_a}{k_B T}\right) \\ &= \sigma_0 \exp\left(\frac{E_a^{\text{eff}}}{k_B T}\right) \end{aligned} \quad (1)$$

where  $Z_i$  is the ionic charge,  $N_A$  is the Avogadro constant,  $C_{v0}$  is the concentration of intrinsic defects,  $D_0$  is the diffusion coefficient,  $V_m$  is the molar volume of perovskite,  $G_v$  is the formation energy for vacancy defects,  $k_B$  is Boltzmann's constant, and the activation energy for ion migration  $E_a^{\text{eff}}$  could be derived from the slope of the  $\ln(\sigma_{\text{ion}} T) \approx 1/T$  relation.

The total conductivity of the thin film consists of both electrons and ions ( $\sigma_{\text{total}} = \sigma_e + \sigma_{\text{ion}}$ ) because a perovskite is an ionic conductor.  $\sigma_{\text{total}}$  is proportional to the slope of the current–voltage curve with a fast scanning rate ( $50 \text{ V s}^{-1}$ ) in the lateral structure (Figure 2b). Because the scanning period is shorter than 1 s, the ionic accumulation effect can be safely ignored. Next, we use galvanostatic measurement to separate the electronic conductivity  $\sigma_e$  from  $\sigma_{\text{total}}$ .<sup>29,32,33</sup> Upon switching on a sufficiently weak current, the voltage instantaneously reaches an initial value and then gradually increases over time until reaching a plateau (Figure 2c). During this time, the resistance gradually increases due to the depleted mobile ions at the interface. As a consequence, it reaches an equilibrium value because all mobile ions are blocked at the boundary. The equilibrium value is electronic conductance. The desired ionic conductivity is obtained by using  $\sigma_{\text{ion}} = \sigma_{\text{total}} - \sigma_e$ .

We separate the ionic conductivities of  $\text{CsPbI}_2\text{Br}$  (Figure 2d) and  $\text{MAPbI}_3$  films (Figure 2f) under different light intensities ( $0.1$ – $25 \text{ mW/cm}^2$ ).  $\ln(\sigma_{\text{ion}} T)$  should be plotted versus  $1000/T$  based on eq 1, which describes the hopping-like transport of ion migration. The zoom-in activation region reveals distinct linear regions ( $T > 250 \text{ K}$ ) for  $\text{CsPbI}_2\text{Br}$  (Figure 2e) and  $\text{MAPbI}_3$  films (Figure 2f), respectively.  $E_a$  ( $T > 250 \text{ K}$ ) values under different light intensity for  $\text{CsPbI}_2\text{Br}$  and  $\text{MAPbI}_3$  are summarized in Table 1.

**Table 1. Activation Energy for Ion Migration under Various Light Intensities, for  $\text{CsPbI}_2\text{Br}$  and  $\text{MAPbI}_3$  Films**

light intensity ( $\text{mW cm}^{-2}$ )	$E_{a1}$ for $\text{MAPbI}_3$ ( $T > 250 \text{ K}$ ) (meV)	$E_{a1}$ for $\text{CsPbI}_2\text{Br}$ ( $T > 250 \text{ K}$ ) (meV)
0.1	622	454
5	144	456
25	70	430

The ion migration barrier ( $E_a$ ) in  $\text{MAPbI}_3$  films presents a striking decrease from 0.62 to 0.07 eV when the light intensity changes from 0.1 to  $25 \text{ mW/cm}^2$ . The much lower barrier for ion migration under stronger light will cause more severe ion migration in  $\text{MAPbI}_3$  film, leading to a fast burn-in degradation of solar cells.<sup>10,19,30,34,35</sup> In contrast,  $E_a$  in  $\text{CsPbI}_2\text{Br}$  remains constant under different light intensity (0.45–0.43 eV), revealing the light-independent  $E_a$  of  $\text{CsPbI}_2\text{Br}$  perovskite. The elimination of

light-enhanced ion migration by Cs substitution highlights the key role that an organic cation plays in the complicated interplay between photon excitation and ionic transport. Gottesman et al. demonstrates a softer lattice of  $\text{MAPbI}_3$  perovskites under illumination, arising from reduced binding between the  $\text{MA}^+$  ions and the inorganic frames, which might be a contributing factor for the light-enhanced ion migration.<sup>36</sup> Recently, polaron formation with a deformed lattice surrounding the photocarriers has been demonstrated in  $\text{MA/FAPbBr}_3$  while not in  $\text{CsPbBr}_3$ .<sup>37</sup> The organic cation-dependent polaron formation matches well with cation-dependent ionic transport properties, implying another potential mechanism for light-enhanced ion migration.<sup>38</sup>

We further move on to examine halide segregation in Cs-based perovskite films under laser excitation. Light-induced halide segregation has been widely demonstrated in  $\text{MAPb(I}_x\text{Br}_{1-x})_3$  ( $0.2 < x < 0.9$ ) perovskite films, which can be explained by light-enhanced ion migration.<sup>30,31,38</sup> We investigate the photoluminescence (PL) behavior of  $\text{CsPbI}_2\text{Br}$  and  $\text{CsPbBr}_2\text{I}$  perovskite films on an  $\text{Al}_2\text{O}_3$  substrate. The initial PL spectra show a 645 nm peak (1.92 eV) for  $\text{CsPbI}_2\text{Br}$  (Figure 3a) and a 602 nm peak (2.06 eV) for  $\text{CsPbBr}_2\text{I}$  (Figure 3b). No peak shift is observed after 4 min of light soaking ( $\sim 10^4 \text{ mW/cm}^2$ ). A zoom-in view shows only a monotonic decrease of PL intensity (Figure S4). Additionally, during the same period of light soaking,  $\text{CsPbBr}_2\text{I}$  shows a higher stability of PL intensity, and it can be explained by its better phase stability compared to that of  $\text{CsPbI}_2\text{Br}$  in ambient air conditions.<sup>20,22,23</sup> The suppressed photoinduced phase segregation in cesium lead halide perovskites, in turn, supports the light-independent ion migration property. Note that in  $\text{MAPb(I}_{0.5}\text{Br}_{0.5})_3$  the initial PL peak red shifts immediately once the laser is applied on the sample less than 1 ms (Figure 3c).

On the basis of the analysis above, we infer that the PSCs based on Cs-perovskite should achieve better MPP stability than MA-perovskite PSCs because the built-in electric field can barely move the ions in Cs-perovskites under illumination. To fabricate the  $\text{CsPbI}_2\text{Br}$  film, mixed solvent (DMSO/DMF) is used here to increase the precursor solubility to 0.83 M. The resulting film exhibits dense morphology with 10.8 nm roughness, large grain size (1–2  $\mu\text{m}$ ), and 300 nm thickness (Figure 4). The X-ray diffraction (XRD) pattern confirms the cubic structure of a pure  $\text{CsPbI}_2\text{Br}$  polycrystalline film on *c*- $\text{TiO}_2$  with two main peaks at 14.7 and 29.6° (Figure S5a). Compared to a pure DMF solvent with 0.4 M limited solubility, mixed solvent improves not only the film morphology and thickness (Figure S6) but the resulting absorption (Figure S5b). The enhancement in the long-wavelength region (500–650 nm) indicates a thicker film from the 0.83 M (DMF/DMSO) precursor solution.

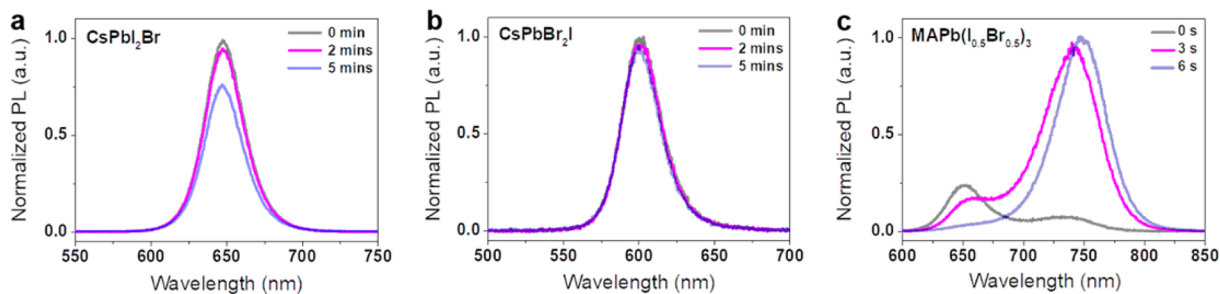


**Figure 3.** PL spectra for perovskite films on alumina substrates at  $10^4 \text{ mW/cm}^2$  intensity measured in ambient air. (a)  $\text{CsPbI}_2\text{Br}$  films measured at 2 min intervals. (b)  $\text{CsPbBr}_2\text{I}$  films measured at 2 min intervals. (c)  $\text{MAPb(I}_{0.5}\text{Br}_{0.5})_3$  measured at 3 s intervals.

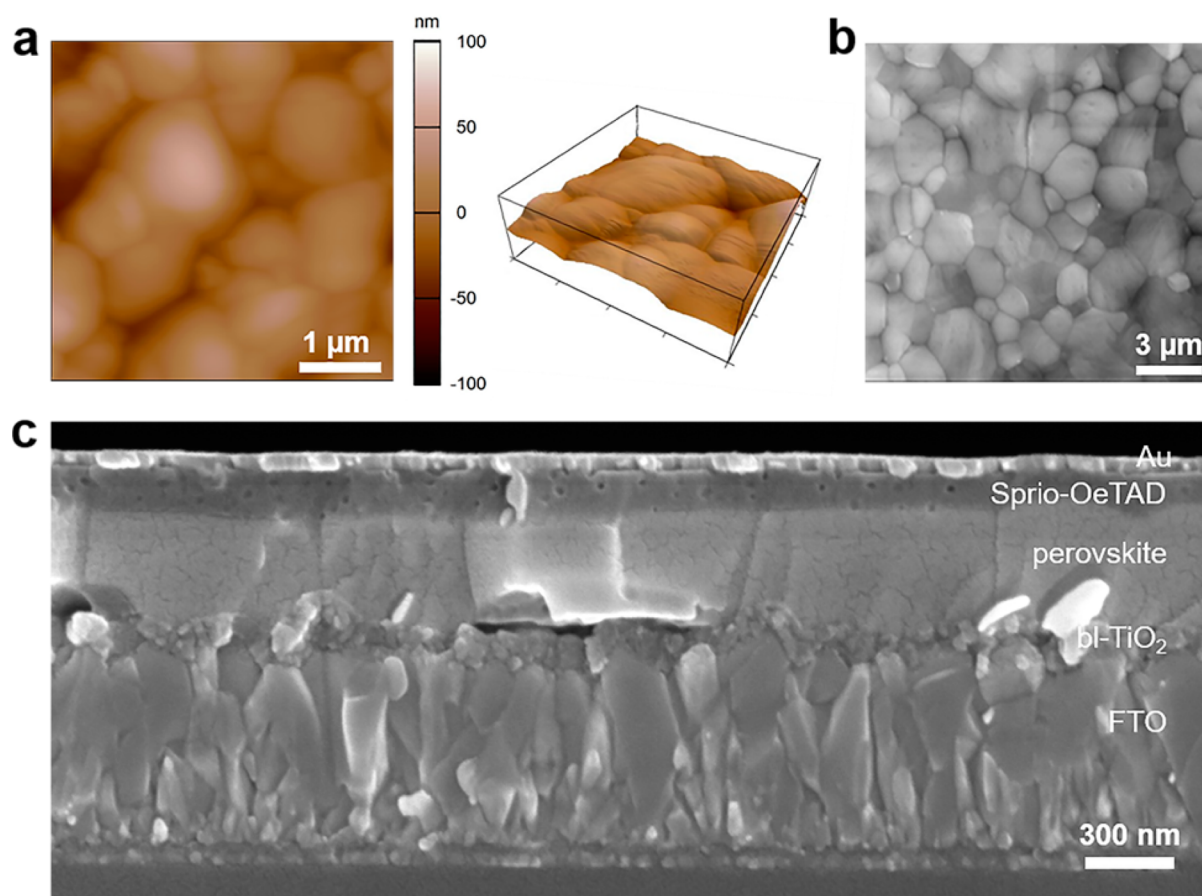


**Figure 4.** AFM and SEM images of CsPbI<sub>2</sub>Br layers fabricated by antisolvent methods from a 0.83 M (DMF/DMSO) precursor solution. (a) AFM topography (left) and three-dimensional views (right). (b) Top-view SEM image of the perovskite layer on a TiO<sub>2</sub> film. (c) Cross-sectional SEM image of a complete perovskite device.

CsPbI<sub>2</sub>Br solar cells show an improved average PCE over 8.2% (Figure S7) with a 10.3% champion PCE (Figure 5a). The final steady-state power output at MPP tracking is 9.3% (Figure S8).

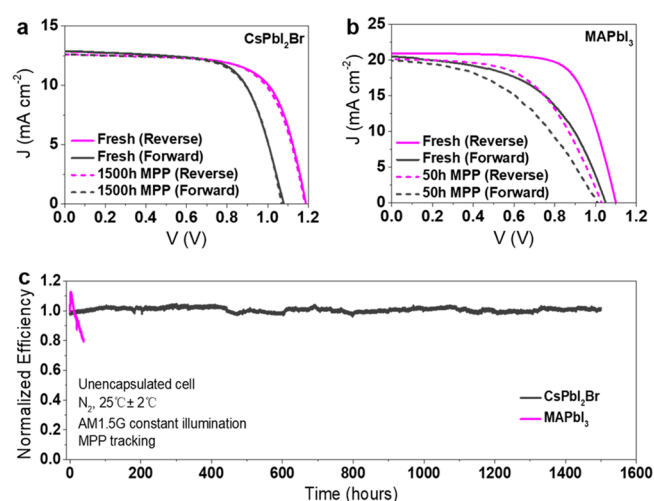


**Figure 5.** Photovoltaic performance and long-term stability of PSCs.  $J$ - $V$  scans of (a) CsPbI<sub>2</sub>Br and (b) MAPbI<sub>3</sub> PSCs at various stages: fresh and right after corresponding MPP operation. The  $J$ - $V$  curves were measured without a UV filter. (c) Continuous maximum point tracking for over 1500 h of the unsealed champion CsPbI<sub>2</sub>Br (dark gray line) and MAPbI<sub>3</sub> solar cells (magenta line) in a nitrogen glovebox (25 °C) under constant AM1.5G illumination with a 420 nm UV filter.

We also note a significant hysteresis in  $J$ - $V$  scan measurements for devices, similar to other reported CsPbI<sub>2</sub>Br solar cells.<sup>23,39</sup>

It may relate to the interfacial defects between the compact TiO<sub>2</sub> and perovskite layer.<sup>5,40,41</sup> To compare our stability with previous results,<sup>3,5,6</sup> we filtered the UV part in the AM1.5G spectrum for the MPP stability test, as shown in Figure 5c. On the basis of the long-term stability evaluation, the Cs-perovskite device exhibits negligible efficiency loss in 1500 h under continuous light illumination and steady-state measurement at the MPP in an inert environment, compared to 50 h for the MAPbI<sub>3</sub> device. We also monitored the stability with a full AM1.5G spectrum, showing comparable stable performance in the first 40 h (Figure S9). The  $J$ - $V$  performances for CsPbI<sub>2</sub>Br and MAPbI<sub>3</sub> PSC at different stages are also shown in Figure 5a,b. This result demonstrates the longest operational stability of Cs-PSCs. It, in turn, supports the superior intrinsic stability of the CsPbI<sub>2</sub>Br film and demonstration of a light-independent barrier for ion migration.

In the recent development of lead halide PSCs, devices containing mixed A-site organic cations (MA and FA with little Cs component) exhibited record efficiency and long-term stability. However, efficiency loss under operational status still exists after periods of working under light, and light-enhanced ion migration via a MA cation may be the origin. In order to improve the stability of PSCs, future investigation should be focused on finding the phase-stable perovskite composition with a minimized organic cation to retain the high stability. Moreover, the CsPbI<sub>2</sub>Br material has a promising prospect for application in

tandem-top solar cells. Therefore, it preserves a bright future in PSC development.

Overall, light-dependent ion migration is quantitatively investigated in CsPbI<sub>2</sub>Br and MAPbI<sub>3</sub> films by separating electronic and ionic conductivities. Unlike light-enhanced ion migration in MAPbI<sub>3</sub>, we find that the activation energy for ion migration of the CsPbI<sub>2</sub>Br sample is constant (~0.45 eV) under different light intensity. This property of cesium perovskite is very important for photostability behaviors, including the elimination of halide segregation in cesium perovskite films and the potential for device long-term stability. Finally, with solvent-engineering technology, we fabricated condense and uniform CsPbI<sub>2</sub>Br layers and demonstrated a solution-processed PSC with 9.3% stable PCE. These planar inorganic PSCs exhibit tremendous improvement on long-term stability under continuous steady-state operation, in comparison to its MA counterpart, showing 1500 h stability under continuous light illumination at MPP tracking. We expect that our findings could boost the investigation of the microscopic mechanism of the optoelectronic properties of photoexcited perovskite materials and push forward the development of stable inorganic PSCs with higher photovoltaic performance.

## EXPERIMENTAL METHODS

**Perovskite Solar Cell Fabrication.** CsPbI<sub>2</sub>Br was prepared from a CsBr/PbI<sub>2</sub> (Alfa Aesar) (1:1) precursor solution. For the 0.4 M precursor solution, CsBr and PbI<sub>2</sub> were dissolved in *N,N*-dimethylformamide (DMF, Sigma-Aldrich). For the 0.83 M precursor solution, CsBr and PbI<sub>2</sub> were dissolved in DMF with an additional 56.8  $\mu$ L of dimethyl sulfoxide (DMSO, Sigma-Aldrich). All of the precursor solutions were prepared under an inert atmosphere in an N<sub>2</sub> glovebox with <0.1 ppm of H<sub>2</sub>O and O<sub>2</sub>, dissolved at 55 °C for 1 h and filtered through a 0.2  $\mu$ m PTFE filter. The 0.83 M precursor solution was deposited onto plasma-cleaned FTO/TiO<sub>2</sub> substrates with two-step spin-coating procedures. The first step was 2000 rpm for 10 s with an acceleration of 200 rpm/s. The second step was 2000 rpm for 40 s. Chlorobenzene (150  $\mu$ L) was dropped on the spinning substrate at 10 s before the end of the second step. The deposition process of the 0.4 M precursor solution followed the same procedure without the chlorobenzene dropping. The films were sintered at 280 °C for 8 min. A 2,2',7,7'-tetrakis(*N,N*-di-4-methoxyphenylamino)-9,9'-spirobifluorene (spiro-OMeTAD, Yingkou OPV Tech New Energy Co., Ltd.) solution was spin-coated on perovskite/bl-TiO<sub>2</sub>/FTO/glass at 3000 rpm for 50 s to form a hole transporting layer. To prepare a spiro-OMeTAD solution, spiro-OMeTAD/chlorobenzene (72.3 mg/mL, Sigma-Aldrich) was mixed with 17.5  $\mu$ L of lithium bis(trifluoromethanesulfonyl)imide/acetonitrile (520 mg/mL, both from Sigma-Aldrich) and 28.8  $\mu$ L of 4-*tert*-butylpyridine (Sigma-Aldrich). Finally, a gold counter electrode was deposited by thermal evaporation. The active electrode area was fixed at 9 mm<sup>2</sup>.

**Perovskite Films and Solar Cell Characterization.** The surface morphology of the perovskite thin film and cross section of the solar cell devices were characterized by scanning electron microscopy (SEM) (Nano430, FEI). The instrument uses an electron beam accelerated at 5 kV. AFM was performed using Asylum Research/MFP-3D in tapping mode. PL spectra were measured using a green laser (532 nm in wavelength) on a micro-zone confocal Raman spectroscope (Renishaw inVia microRaman system). The laser beam had a spot size diameter of 2  $\mu$ m.

Optical absorption measurements were carried out in a Lambda 950 UV/vis spectrophotometer.

The current–voltage (*J–V*) curves were obtained by an Agilent B2912 Series precision source/measure unit and a solar simulator (Solar IV-150A, Zolix). Light intensity was calibrated with a Newport calibrated KG5-filtered Si reference cell. A black mask was used to define the cells' area. The *J–V* curves were tested from 1.5 to –0.2 V with a scan velocity of 100 mV/s (voltage step of 10 mV and delay time of 200 ms). For the steady-state efficiency, PCE(*t*) was measured by setting the bias voltage to the *V*<sub>MPP</sub> and then tracing the current density in a nitrogen-filled glovebox without encapsulation (~20% RH). The long-term stability test at continuous MPP conditions and 1 sun, AM1.5G illumination was carried out in a nitrogen-filled glovebox at a constant device temperature of 25 °C by setting the bias voltage to *V*<sub>MPP</sub> and tracking the current output. The MPP was updated every 10 s by measuring the current response to a small perturbation in the potential. A 420 nm cutoff UV filter was applied in front of the solar cells during the MPP tracking tests.

**Perovskite Film Fabrication in the Au/Perovskite/Au Lateral Structure.** The thickness of the gold electrodes was approximately 0.1  $\mu$ m, and the gap between the two gold electrodes was 30  $\mu$ m. For CsPbI<sub>2</sub>Br, a 0.83 M CsPbI<sub>2</sub>Br precursor solution (CsBr/PbI<sub>2</sub> (Sigma-Aldrich) (1:1) in DMF with an additional 56.8  $\mu$ L of DMSO) was spin-coated onto the silicon oxide substrate, followed by annealing at 280 °C for 8 min in a glovebox. MAPbBr<sub>3</sub> and MAPb(I<sub>0.9</sub>Br<sub>0.1</sub>)<sub>3</sub> films were prepared from a precursor solution (MABr and MAI/PbAc<sub>2</sub> (Sigma-Aldrich) (3:1)) (annealed at 100 °C for 10 min in the glovebox). Then, 100 nm PMMA was spin-coated on all of the perovskite films.

For details of the electrical measurements in the lateral structure, please refer to ref 30.

## ASSOCIATED CONTENT

### Supporting Information

The Supporting Information is available free of charge on the ACS Publications website at DOI: 10.1021/acs.jpcllett.7b01851.

Experimental apparatus used in the experiments with a helium cooling system; SEM image of a CsPbI<sub>2</sub>Br film in the lateral structure; optical dynamic images of MAPbBr<sub>3</sub> and MAPb(I<sub>0.9</sub>Br<sub>0.1</sub>)<sub>3</sub> films under electric poling and illumination of various intensities; zoomed-in view of the PL spectra for CsPbI<sub>2</sub>Br and CsPbBr<sub>2</sub>I films; XRD patterns and absorbance spectra of CsPbI<sub>2</sub>Br films; AFM and SEM images of CsPbI<sub>2</sub>Br layers fabricated by a one-step process; histograms of the *J–V* scan efficiencies for CsPbI<sub>2</sub>Br devices; stabilized maximum power output; and the photocurrent density at the maximum power point as a function of time for the best-performing CsPbI<sub>2</sub>Br PSC (PDF)

## AUTHOR INFORMATION

### Corresponding Author

\*E-mail: zhaoping@pku.edu.cn.

### ORCID

Qing Zhao: 0000-0003-3374-6901

### Author Contributions

#Contributed equally to this work.

### Notes

The authors declare no competing financial interest.

## ACKNOWLEDGMENTS

This work was supported by National 973 projects (2013CB932602, MOST) from the Ministry of Science and Technology, China, the National Natural Science Foundation of China (NSFC 51622201, 61571015, 91433102, 11327902, 11234001, and 51522201), and the National Key Research and Development Program of China (No. 2016YFA0300802, 2016YFA0300903).

## REFERENCES

- (1) Yang, W. S.; Park, B.-W.; Jung, E. H.; Jeon, N. J.; Kim, Y. C.; Lee, D. U.; Shin, S. S.; Seo, J.; Kim, E. K.; Noh, J. H.; et al. Iodide management in formamidinium-lead-halide-based perovskite layers for efficient solar cells. *Science* **2017**, *356*, 1376–1379.
- (2) Yang, W. S.; Noh, J. H.; Jeon, N. J.; Kim, Y. C.; Ryu, S.; Seo, J.; Seok, S. I. High-performance photovoltaic perovskite layers fabricated through intramolecular exchange. *Science* **2015**, *348*, 1234–1237.
- (3) Saliba, M.; Matsui, T.; Seo, J.-Y.; Domanski, K.; Correa-Baena, J.-P.; Nazeeruddin, M. K.; Zakeeruddin, S. M.; Tress, W.; Abate, A.; Hagfeldt, A.; et al. Cesium-containing triple cation perovskite solar cells: improved stability, reproducibility and high efficiency. *Energy Environ. Sci.* **2016**, *9*, 1989–1997.
- (4) Saliba, M.; Matsui, T.; Domanski, K.; Seo, J.-Y.; Ummadisingu, A.; Zakeeruddin, S. M.; Correa-Baena, J.-P.; Tress, W. R.; Abate, A.; Hagfeldt, A.; et al. Incorporation of rubidium cations into perovskite solar cells improves photovoltaic performance. *Science* **2016**, *354*, 206–209.
- (5) Tan, H.; Jain, A.; Voznyy, O.; Lan, X.; García de Arquer, F. P.; Fan, J. Z.; Quintero-Bermudez, R.; Yuan, M.; Zhang, B.; Zhao, Y.; et al. Efficient and stable solution-processed planar perovskite solar cells via contact passivation. *Science* **2017**, *355*, 722–726.
- (6) Shin, S. S.; Yeom, E. J.; Yang, W. S.; Hur, S.; Kim, M. G.; Im, J.; Seo, J.; Noh, J. H.; Seok, S. I. Colloidally prepared La-doped BaSnO<sub>3</sub> electrodes for efficient, photostable perovskite solar cells. *Science* **2017**, *356*, 167–171.
- (7) Eperon, G. E.; Leijtens, T.; Bush, K. A.; Prasanna, R.; Green, T.; Wang, J. T.-W.; McMeekin, D. P.; Volonakis, G.; Milot, R. L.; May, R.; Palmstrom, A.; et al. Perovskite-perovskite tandem photovoltaics with optimized band gaps. *Science* **2016**, *354*, 861–865.
- (8) Bella, F.; Griffini, G.; Correa-Baena, J.-P.; Saracco, G.; Grätzel, M.; Hagfeldt, A.; Turri, S.; Gerbaldi, C. Improving efficiency and stability of perovskite solar cells with photocurable fluoropolymers. *Science* **2016**, *354*, 203–206.
- (9) Xiao, Z.; Yuan, Y.; Shao, Y.; Wang, Q.; Dong, Q.; Bi, C.; Sharma, P.; Gruverman, A.; Huang, J. Giant switchable photovoltaic effect in organometal trihalide perovskite devices. *Nat. Mater.* **2014**, *14*, 193–198.
- (10) Leijtens, T.; Hoke, E. T.; Grancini, G.; Slotcavage, D. J.; Eperon, G. E.; Ball, J. M.; De Bastiani, M.; Bowring, A. R.; Martino, N.; Wojciechowski, K.; et al. Stability of metal halide perovskite solar cells. *Adv. Energy Mater.* **2015**, *5*, 1500963.
- (11) Yuan, Y.; Chae, J.; Shao, Y.; Wang, Q.; Xiao, Z.; Centrone, A.; Huang, J. Photovoltaic switching Mechanism in lateral structure hybrid perovskite solar cells. *Adv. Energy Mater.* **2015**, *5*, 1500615.
- (12) Yuan, Y.; Wang, Q.; Shao, Y.; Lu, H.; Li, T.; Gruverman, A.; Huang, J. Electric-field-driven reversible conversion between methylammonium lead triiodide perovskites and lead iodide at elevated temperatures. *Adv. Energy Mater.* **2016**, *6*, 1501803.
- (13) Zhao, Y.; Wei, J.; Li, H.; Yan, Y.; Zhou, W.; Yu, D.; Zhao, Q. A polymer scaffold for self-healing perovskite solar cells. *Nat. Commun.* **2016**, *7*, 10228.
- (14) Zhao, Y.; Zhou, W.; Ma, W.; Meng, S.; Li, H.; Wei, J.; Fu, R.; Liu, K.; Yu, D.; Zhao, Q. Correlations between immobilizing ions and suppressing hysteresis in perovskite solar cells. *ACS Energy Lett.* **2016**, *1*, 266–272.
- (15) Yuan, H.; Debroye, E.; Janssen, K.; Naiki, H.; Steuwe, C.; Lu, G.; Moris, M.; Orgiu, E.; Uji-i, H.; De Schryver, F.; et al. Degradation of methylammonium lead iodide perovskite structures through light and electron beam driven ion migration. *J. Phys. Chem. Lett.* **2016**, *7*, 561–566.
- (16) Bae, S.; Kim, S.; Lee, S.-W.; Cho, K. J.; Park, S.; Lee, S.; Kang, Y.; Lee, H.-S.; Kim, D. Electric-field-induced degradation of methylammonium lead iodide perovskite solar cells. *J. Phys. Chem. Lett.* **2016**, *7*, 3091–3096.
- (17) Bag, M.; Renna, L. A.; Adhikari, R. Y.; Karak, S.; Liu, F.; Lahti, P. M.; Russell, T. P.; Tuominen, M. T.; Venkataraman, D. Kinetics of ion transport in perovskite active layers and its implications for active layer stability. *J. Am. Chem. Soc.* **2015**, *137*, 13130–13137.
- (18) Yun, J. S.; Seidel, J.; Kim, J.; Soufiani, A. M.; Huang, S.; Lau, J.; Jeon, N. J.; Seok, S. I.; Green, M. A.; Ho-Baillie, A. Critical role of grain boundaries for ion migration in formamidinium and methylammonium lead halide perovskite solar cells. *Adv. Energy Mater.* **2016**, *6*, 1600330.
- (19) Domanski, K.; Roose, B.; Matsui, T.; Saliba, M.; Turren-Cruz, S.-H.; Correa-Baena, J.-P.; Carmona, C. R.; Richardson, G.; Foster, J. M.; De Angelis, F.; et al. Migration of cations induces reversible performance losses over day/night cycling in perovskite solar cells. *Energy Environ. Sci.* **2017**, *10*, 604–613.
- (20) Leijtens, T.; Bush, K.; Cheacharoen, R.; Beal, R.; Bowring, A.; McGehee, M. D. Towards enabling stable lead halide perovskite solar cells; interplay between structural, environmental, and thermal stability. *J. Mater. Chem. A* **2017**, *5*, 11483–11500.
- (21) Li, Z.; Yang, M.; Park, J.-S.; Wei, S.-H.; Berry, J. J.; Zhu, K. Stabilizing perovskite structures by tuning tolerance factor: formation of formamidinium and cesium lead iodide solid-state alloys. *Chem. Mater.* **2016**, *28*, 284–292.
- (22) Beal, R. E.; Slotcavage, D. J.; Leijtens, T.; Bowring, A. R.; Belisle, R. A.; Nguyen, W. H.; Burkhard, G. F.; Hoke, E. T.; McGehee, M. D. Cesium lead halide perovskites with improved stability for tandem solar cells. *J. Phys. Chem. Lett.* **2016**, *7*, 746–751.
- (23) Sutton, R. J.; Eperon, G. E.; Miranda, L.; Parrott, E. S.; Kamino, B. A.; Patel, J. B.; Hörantner, M. T.; Johnston, M. B.; Haghighirad, A. A.; Moore, D. T.; et al. Bandgap-tunable cesium lead halide perovskites with high thermal stability for efficient solar cells. *Adv. Energy Mater.* **2016**, *6*, 1502458.
- (24) McMeekin, D. P.; Sadoughi, G.; Rehman, W.; Eperon, G. E.; Saliba, M.; Hörantner, M. T.; Haghighirad, A.; Sakai, N.; Korte, L.; Rech, B.; et al. A mixed-cation lead mixed-halide perovskite absorber for tandem solar cells. *Science* **2016**, *351*, 151–155.
- (25) Lee, J.-W.; Kim, D.-H.; Kim, H.-S.; Seo, S.-W.; Cho, S. M.; Park, N.-G. Formamidinium and cesium hybridization for photo- and moisture-stable perovskite solar cell. *Adv. Energy Mater.* **2015**, *5*, 1501310.
- (26) Eperon, G. E.; Paterno, G. M.; Sutton, R. J.; Zampetti, A.; Haghighirad, A. A.; Cacialli, F.; Snaith, H. J. Inorganic caesium lead iodide perovskite solar cells. *J. Mater. Chem. A* **2015**, *3*, 19688–19695.
- (27) Liang, J.; Wang, C.; Wang, Y.; Xu, Z.; Lu, Z.; Ma, Y.; Zhu, H.; Hu, Y.; Xiao, C.; Yi, X.; et al. All-inorganic perovskite solar cells. *J. Am. Chem. Soc.* **2016**, *138*, 15829–15832.
- (28) Yang, T.-Y.; Gregori, G.; Pellet, N.; Grätzel, M.; Maier, J. The significance of ion conduction in a hybrid organic–inorganic lead-iodide-based perovskite photosensitizer. *Angew. Chem.* **2015**, *127*, 8016–8021.
- (29) Yokota, I. On the theory of mixed conduction with special reference to conduction in silver sulfide group semiconductors. *J. Phys. Soc. Jpn.* **1961**, *16*, 2213–2223.
- (30) Zhao, Y.; Zhou, W.; Zhou, X.; Liu, K.; Yu, D.; Zhao, Q. Quantification of light-enhanced ionic transport in lead iodide perovskite thin films and its solar cell applications. *Light: Sci. Appl.* **2016**, *6*, e16243.
- (31) Hoke, E. T.; Slotcavage, D. J.; Dohner, E. R.; Bowring, A. R.; Karunadasa, H. I.; McGehee, M. D. Reversible photo-induced trap formation in mixed-halide hybrid perovskites for photovoltaics. *Chem. Sci.* **2015**, *6*, 613–617.
- (32) Mizusaki, J.; Arai, K.; Fueki, K. Ionic conduction of the perovskite-type halides. *Solid State Ionics* **1983**, *11*, 203–211.
- (33) Yokota, I. On the electrical conductivity of cuprous sulfide: a diffusion theory. *J. Phys. Soc. Jpn.* **1953**, *8*, 595–602.

(34) Eames, C.; Frost, J. M.; Barnes, P. R. F.; O'Regan, B. C.; Walsh, A.; Islam, M. S. Ionic transport in hybrid lead iodide perovskite solar cells. *Nat. Commun.* **2015**, *6*, 7497.

(35) Brenner, T. M.; Egger, D. A.; Kronik, L.; Hodes, G.; Cahen, D. Hybrid organic–inorganic perovskites: low-cost semiconductors with intriguing charge-transport properties. *Nat. Rev. Mater.* **2016**, *1*, 15007.

(36) Gottesman, R.; Gouda, L.; Kalanoor, B. S.; Haltzi, E.; Tirosh, S.; Rosh-Hodesh, E.; Tischler, Y.; Zaban, A.; Quarti, C.; Mosconi, E.; et al. Photoinduced reversible structural transformations in free-standing  $\text{CH}_3\text{NH}_3\text{PbI}_3$  perovskite films. *J. Phys. Chem. Lett.* **2015**, *6*, 2332–2238.

(37) Zhu, H.; Miyata, K.; Fu, Y.; Wang, J.; Joshi, P. P.; Niesner, D.; Williams, K. W.; Jin, S.; Zhu, X.-Y. Screening in crystalline liquids protects energetic carriers in hybrid perovskites. *Science* **2016**, *353*, 1409–1413.

(38) Bischak, C. G.; Hetherington, C. L.; Wu, H.; Aloni, S.; Ogletree, D. F.; Limmer, D. T.; Ginsberg, N. S. Origin of reversible photoinduced phase separation in hybrid perovskites. *Nano Lett.* **2017**, *17*, 1028–1033.

(39) Nam, J. K.; Chai, S. U.; Cha, W.; Choi, Y. J.; Kim, W.; Jung, M. S.; Kwon, J.; Kim, D.; Park, J. H. Potassium incorporation for enhanced performance and stability of fully inorganic cesium lead halide perovskite solar cells. *Nano Lett.* **2017**, *17*, 2028–2033.

(40) Tao, C.; Neutzner, S.; Colella, L.; Marras, S.; Srimath Kandada, A. R.; Gandini, M.; Bastiani, M. D.; Pace, G.; Manna, L.; Caironi, M.; et al. 17.6% stabilized efficiency in low-temperature processed planar perovskite solar cells. *Energy Environ. Sci.* **2015**, *8*, 2365–2370.

(41) Belisle, R. A.; Nguyen, W. H.; Bowring, A. R.; Calado, P.; Li, X.; Irvine, S. J. C.; McGehee, M. D.; Barnes, P. R. F.; O'Regan, B. C. Interpretation of inverted photocurrent transients in organic lead halide perovskite solar cells: proof of the field screening by mobile ions and determination of the space charge layer widths. *Energy Environ. Sci.* **2017**, *10*, 192–204.